

## NUMERICAL AND EXPERIMENTAL STUDIES OF MHD FLOW IN A RECTANGULAR DUCT WITH A NON-CONDUCTING FLOW INSERT

*S. Smolentsev*<sup>1</sup>, *Z. Xu*<sup>2</sup>, *Ch. Pan*<sup>2</sup>, *M. Abdou*<sup>1</sup>

<sup>1</sup> *University of California, Los Angeles, USA*

<sup>2</sup> *Southwestern Institute of Physics, China*

We consider magnetohydrodynamic (MHD) flows in a conducting rectangular duct with a non-conducting flow channel insert (FCI) in a constant transverse magnetic field. The computations based on the fully developed flow model are performed for three FCI modifications: (i) without pressure equalization openings, (ii) with the pressure equalization slot (PES) in the FCI wall parallel and (iii) perpendicular to the applied magnetic field. The computed flow patterns and the current circuits in the duct with the FCI are analyzed. The experiments are performed with In-Ga-Sn as a work fluid flowing in an outer rectangular duct made of stainless steel with the FCI made of epoxy for two cases: FCI with the PES, and with the pressure equalization holes (PEH), both made in the FCI wall parallel to the magnetic field. The experiments have confirmed significant reduction of the MHD pressure drop due to the flow insert (larger reduction in the case of PEH) compared to the non-insulated duct, but the experimental MHD pressure drop is different (larger) than the computed one. This difference is discussed and further modifications of both the flow model and the experiment are suggested.

**1. Introduction.** A flow channel insert (FCI) [1] made of silicon carbide (SiC), either composite or foam, is the key element in the US dual-coolant lead-lithium (DCLL) blanket concept [2,3], where it serves as an electrical insulator to reduce the magnetohydrodynamic (MHD) pressure drop, and as a thermal insulator to minimize heat losses into the cooling helium (He) flows, and also to isolate the ferritic (Fe) wall from the hot lead-lithium (PbLi).

In the typical DCLL blanket design [3], the FCI (Fig. 1) is separated from the Fe wall by a thin ( $\sim 2$  mm) gap also filled with PbLi. Both the gap flow and that inside the FCI box (bulk flow) are driven by the same pressure head. The gap and

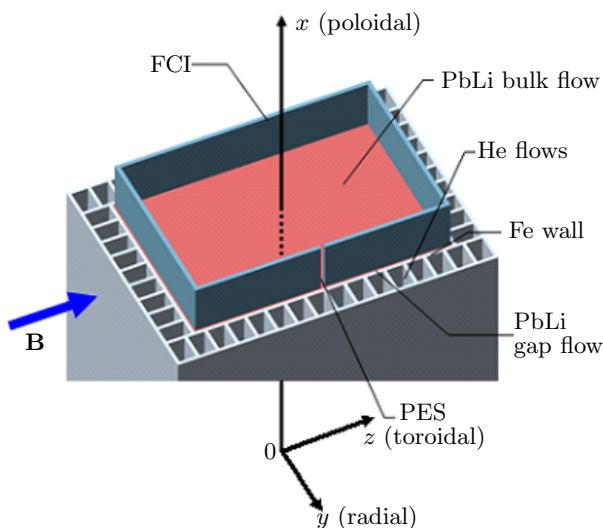


*Fig. 1.* Sketch of the poloidal duct with FCI in the DCLL blanket.

the bulk flows can be connected through small openings made in one of the FCI walls (either holes or a slot). The optimum location of the openings has been analyzed in [4]. The openings may be needed for equalizing the pressure on both sides of the FCI, and regarding their shape are referred to as either pressure equalization holes (PEH) or pressure equalization slot (PES). The blanket thermal efficiency is strongly dependent on the FCI insulating properties (electrical and thermal). In the DCLL blanket, the desirable blanket configuration requires minimization of heat leakages from the PbLi flows into He streams as well as minimization of the MHD pressure drop, while keeping the interface temperature between the PbLi and the Fe structure and the temperature drop across the FCI below the allowable limits. Meeting all these requirements places special limitations on the FCI design and SiC properties, such as electrical ( $\sigma_{\text{FCI}}$ ) and thermal ( $k_{\text{FCI}}$ ) conductivity as discussed in [4] and [5]. In this paper, we analyze an MHD flow in a conducting rectangular duct with an insulating flow insert under isothermal conditions in a particular case when the FCI material is a perfect electrical insulator ( $\sigma_{\text{FCI}} \rightarrow 0$ ), which means that there is no any electric currents passing through the FCI walls, but leaking currents from the bulk flow into the gap are still possible through the pressure equalization openings. Although such a case represents idealized conditions when the MHD pressure drop is minimized, in practice, having an ideally insulating FCI may not be optimal as the requirements on the FCI in the real blanket environment are often competing. Nevertheless, from the theoretical point of view, the case of a perfectly insulating FCI material represents asymptotic conditions when the bulk and gap flows are to major degree decoupled electrically. Therefore, this case can serve as a useful reference for the future studies of MHD flows with the insulating flow insert of finite electrical conductivity. Here, in the theoretical part of the study, we use a fully developed flow model to address numerically three FCI configurations: (i) with no openings, (ii) with PES in one of the walls parallel to the applied magnetic field, and (iii) PES in one of the walls perpendicular to the field. The case with PEH is not considered as it probably requires a full 3D simulation to describe the flow and electric current distributions around each hole. In the experimental study, two FCI modifications are used: one with PES and the other one with PEH. In both experimental cases, the pressure equalization openings are located in the FCI wall parallel to the magnetic field. Although a few theoretical studies have already been performed for the flows with FCI (additionally to [4] and [5], see also [6] and [7]), to our knowledge there are only two experimental studies [8, 9]. In [8], experiments were performed to prove the assumption that the FCI could reduce the MHD pressure drop in a circular pipe using a “sandwich” FCI consisting of a thin inner layer of insulating ceramic paper and two outer layers of stainless steel. These experiments show MHD pressure drop reduction by a factor of nearly 9. The 20% deviation of the experimental results from the theoretical predictions is explained by 3D effects associated with the finite length of the magnet. The experimental data presented in this paper are intentionally limited to the MHD pressure drop. More details, including velocity measurements, can be found in [9] for the FCI with PEH and more experimental results for the PES case will be presented in a separate paper.

The cross-sectional area of the reference duct with a FCI is sketched in Fig. 2, showing also the basic dimensions and the computational mesh. The two relevant dimensionless parameters are the Hartmann and Reynolds numbers:  $\text{Ha} = B_0^z L_* \sqrt{\sigma_1 / (\nu_1 \rho_1)}$  and  $\text{Re} = U_* L_* / \nu_1$ . Here,  $B_0^z$  is the applied transverse magnetic field,  $U_*$  is the characteristic velocity,  $L_*$  is the characteristic dimension of the duct taken along the magnetic field direction, and  $\sigma_1$ ,  $\nu_1$  and  $\rho_1$  are the fluid electric conductivity, kinematic viscosity and density, correspondingly. In the pa-

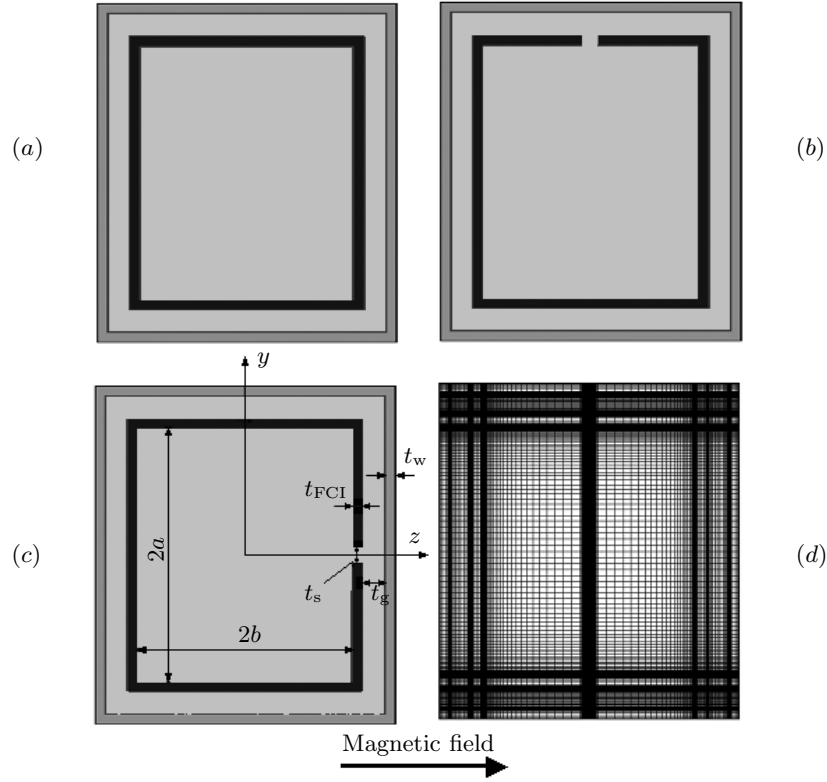


*Fig. 2.* Sketch of the cross-sectional area of the reference MHD flow: (a) no openings in the FCI, (b) slot in the FCI wall parallel to the magnetic field, (c) slot in the FCI wall perpendicular to the magnetic field, and (d) example of the computational mesh for the case (b).

per, we use two Hartmann numbers:  $Ha_1$  is constructed through the half-width of the FCI box, while  $Ha_2$  is based on the similar dimension of the outer electrically conducting duct. The Reynolds number is built using the half-width of the outer duct and the mean bulk velocity  $U_m$  defined as

$$U_m = \frac{1}{S} \iint_S U(z, y) dz dy,$$

where integration is performed over the area  $S$ , including the bulk flow and those in the gap and the pressure equalization slot. The cross-sectional dimensions of the duct with the FCI used in the computations are taken identical to those in the experiment (Table 1). The magnetic field changes from 1 to 2 T. The liquid

*Table 1.* Basic dimensions of the duct with a FCI in experiment and simulations (see also notations in Fig. 2c).

Dimension	Notation	Value, m
Half-width of the FCI box	$b$	0.023
Half-height of the FCI box	$a$	0.027
FCI thickness	$t_{\text{FCI}}$	0.002
Thickness of the gap	$t_g$	0.005
Thickness of the slot	$t_s$	0.003
Thickness of the Fe wall	$t_w$	0.002

metal used in both the experiment and the computational studies is a eutectic alloy In-Ga-Sn (indium-gallium-tin).

**2. Computations.** The numerical code used in this study has been developed in [10]. The mathematical model for fully developed flows includes the momentum and induction equations coupled through the Lorentz force term on the right-hand-side of the momentum equation and the velocity-dependent source term on the right-hand-side of the induction equation:

$$\nu_1 \left( \frac{\partial^2 U}{\partial z^2} + \frac{\partial^2 U}{\partial y^2} \right) - \frac{1}{\rho_1} \frac{dP}{dx} + \frac{1}{\rho_1} j_y B_0^z = 0, \quad (1)$$

$$\frac{1}{\mu_0} \frac{\partial}{\partial z} \left( \frac{1}{\sigma} \frac{\partial B_x}{\partial z} \right) + \frac{1}{\mu_0} \frac{\partial}{\partial y} \left( \frac{1}{\sigma} \frac{\partial B_x}{\partial y} \right) + \frac{1}{\rho_1} \frac{dP}{dx} + B_0^z \frac{\partial U}{\partial z} = 0. \quad (2)$$

Here,  $\mu_0$  is the magnetic permeability of vacuum. The electric conductivity  $\sigma = \sigma_1$  in the bulk flow, gap and in the slot,  $\sigma = \sigma_{\text{FCI}}$  within the flow channel insert, and  $\sigma = \sigma_w$  in the conducting wall. Providing the induced magnetic field  $B_x$  is known, the components of the electric current density vector  $(j_z, j_y)$  can be calculated as

$$j_y = \frac{1}{\mu_0} \frac{\partial B_x}{\partial z}, \quad j_z = -\frac{1}{\mu_0} \frac{\partial B_x}{\partial y}. \quad (3)$$

The induction equation is formulated here in the conservative form, such that the second derivatives are written as  $\frac{\partial}{\partial z} \left( \frac{1}{\sigma} \frac{\partial B_x}{\partial z} \right)$ . Using the conservative formulation allows computations for multi-material domains, including the FCI, liquid metal flows and the external conducting wall without implementation of the inner boundary conditions at the material interfaces, which require matching the magnetic field and the tangential component of the electric field. In doing so, the induction equation is solved over the whole cross-sectional area of the duct in a continuous manner, while the momentum equation is solved only in the areas filled with liquid metal, i.e., inside the FCI box, in the gap and the pressure equalization slot. The boundary condition on the induced magnetic field is formulated at the external surface of the conducting duct, which is  $B_x = 0$ , as the flow is fully developed. The non-uniform meshes used in the computations are Hartmann number sensitive, so that higher resolution in the liquid sub-domains is provided near the walls within the Hartmann and side layers and also within the pressure equalization slot (Fig. 2d). Typical meshes include  $201 \times 201$  grid points within the bulk flow inside the FCI box. Of them, 101 points are located in the slot. There are 51 points in both the gap and the conducting wall. Such a mesh is very fine allowing detailed flow resolution. The solution is obtained via iterations until the residual defined through the dimensionless flowrate as  $|(Q^{n+1} - Q^n)/Q^{n+1}|$  becomes repeatedly smaller than a predefined small number  $\varepsilon \sim 10^{-9}$ . All computations are performed with double precision.

An example of convergence is shown in Fig. 3 for the case without pressure equalization openings at  $\text{Ha}_1 = 959$  ( $B_z^0 = 1$  T). The convergence speed is faster in the area inside the FCI box so that the computational time is mostly affected by the computations in the gap. The difference in the convergence speed in the two flows is related to different electric conductivities: a perfectly insulating boundary in the bulk flow, and a highly conducting external boundary in the gap flow (using the formulation based on the induced magnetic field typically results in much faster computations if the walls are non-conducting or poorly conducting). This results in millions of iterations, as shown in Fig. 3, and requires a few days of computations

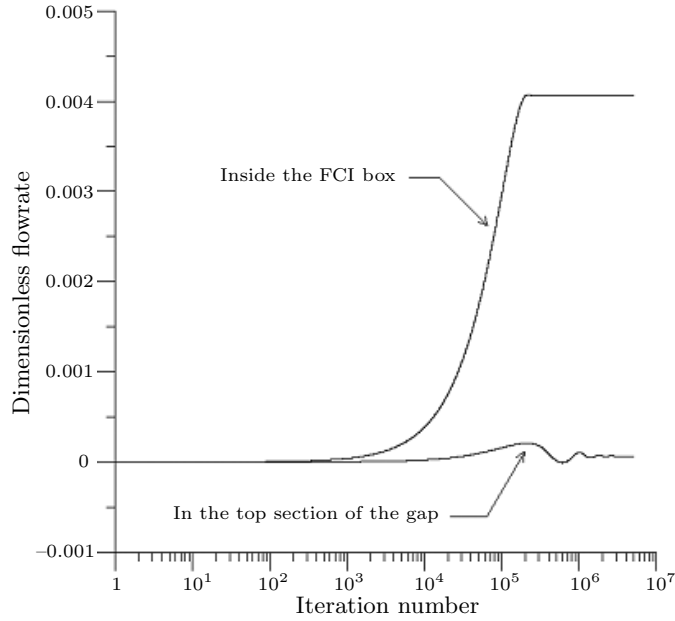


Fig. 3. Convergence of the solution (the case without pressure equalization openings).

using a PC. However, with the relaxation-type acceleration procedure suggested in [10], the number of iterations can be reduced by at least two orders and the computational time drops to just a few hours.

For the validation of the computational results, we also compute the MHD flow in a rectangular duct with ideally insulating walls using the analytical solution by Hunt [11] and compare the obtained results with the numerical computations of the bulk flow inside the perfectly insulating FCI box without any pressure equalization openings. The comparisons are made based on the dimensionless mass flowrate

$$Q_1 = \iint_{S_1} \tilde{U} d\tilde{z} d\tilde{y}$$

as a function of the Hartmann number  $Ha_1$ , which demonstrates a perfect match as seen from Table 2. Here, when taking the integral, the velocity is scaled by  $b^2 \nu_1^{-1} \rho_1^{-1} (-dp/dx)$ , where  $dp/dx$  is the pressure gradient in the flow, and the coordinates are scaled with the dimension  $b$ . Integration is performed over the inner part of the duct cross-sectional area  $S_1$  bounded by the FCI box.

First, the computations are performed for the case with the FCI without pressure equalization openings (Fig. 4). Here, the bulk and gap flows are completely

Table 2. Comparison between the numerical and analytical [11] solutions for the flow inside the ideally insulating flow insert without pressure equalization openings.

$B_0^z, T$	$Ha_1$	$Q_1$ ([10])	$Q_1$ (computations)
1.0	959	$0.4066 \times 10^{-2}$	$0.4061 \times 10^{-2}$
1.3	1246	$0.3138 \times 10^{-2}$	$0.3131 \times 10^{-2}$
1.6	1534	$0.2556 \times 10^{-2}$	$0.2548 \times 10^{-2}$
1.9	1821	$0.2156 \times 10^{-2}$	$0.2149 \times 10^{-2}$

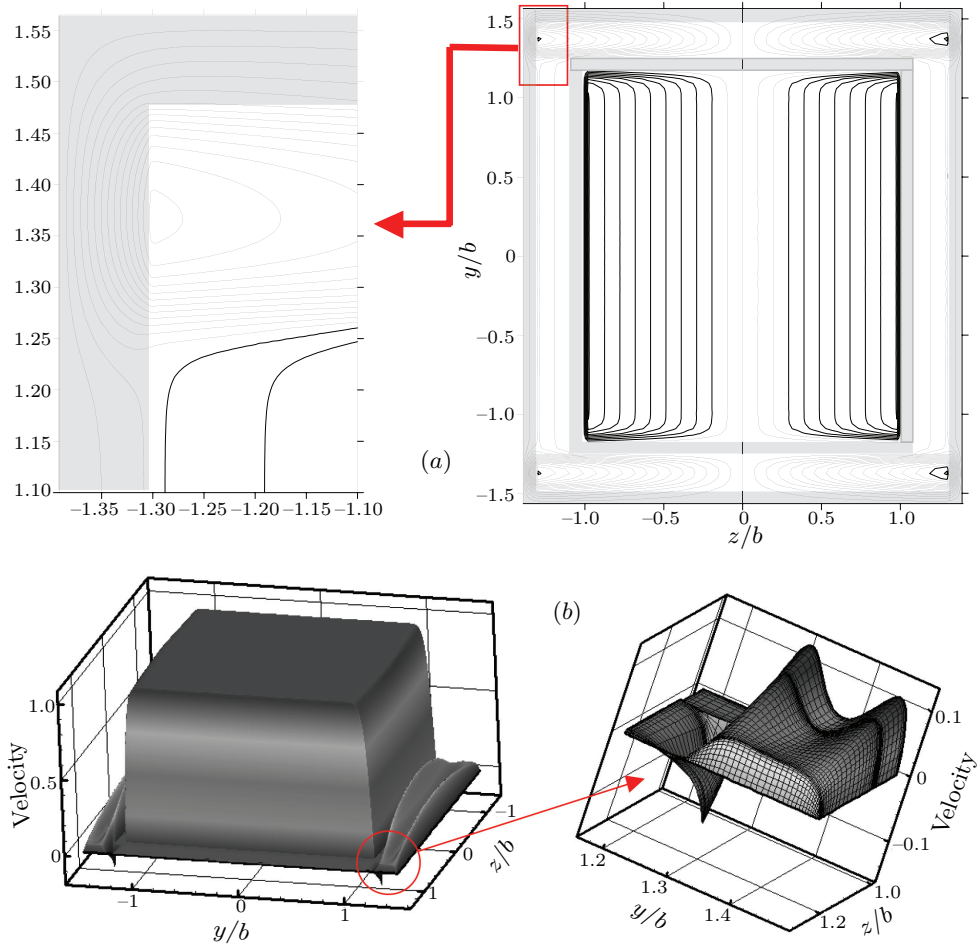


Fig. 4. Computed results for the case of the flow channel insert without pressure equalization openings: (a) induced electric current distribution, and (b) velocity distribution for  $Ha_1 = 959$  ( $B_z^0 = 1$  T).

decoupled. The bulk flow is fully matching the well-known fully developed flow in a non-conducting rectangular duct. Such a flow demonstrates two Hartmann layers with the thickness  $\sim 1/Ha_1$  at the walls perpendicular to the magnetic field, two-side (Shercliff) layers at the walls parallel to the magnetic field with the thickness  $\sim 1/\sqrt{Ha_1}$ , and the uniform velocity core flow. The gap flow demonstrates, however, some special features. Namely, there are four major current loops located in the lower and upper sections of the gap (parallel sections), where the electric current is closed through the electrically conducting walls (Fig. 4a). In each parallel section of the gap, the flow is similar to that in a slotted duct exhibiting an asymmetric “M-shaped” velocity profile (Fig. 4b) with a lower velocity jet at the electrically conducting wall and a higher velocity jet at the opposite wall, which is non-conducting.

The asymmetry in the velocity is related to the difference between the electric conductivity of the FCI and that of the duct so that the current in the parallel gap is asymmetric: the current passing along the FCI wall is completely tangential, while there is a normal current component at the electrically conducting wall giving rise to the Lorentz force that opposes the flow. In the two perpendicular sections,

the flow is almost stagnant. This seems to be caused by the electric currents passing from the corner current loop to the opposite one, which make a closed circuit through the gap and the wall. In the corner regions, where the two gap sections overlap, the flow transients sharply from the “M-shaped” to the stagnant one by forming a negative velocity peak. This peak is very well resolved by the computational mesh as seen in Fig. 4b and, hence, its appearance is not related to any numerical effects associated with the mesh resolution. The transition region between the core flow in the parallel gap and that in the perpendicular one is an example of the internal shear layer. Such free shear layers originating, e.g., from sharp bends in the ducts are well known in magnetohydrodynamics and often referred to as the Ludford layers as they were first identified by Ludford [12], who studied the MHD flow around obstacles (see also [13]). In the case of fully developed flows, such shear layers are fully controlled by the Hartmann number as a result of balancing between electromagnetic and viscous forces, and their thickness is typically proportional to reciprocal of the square root of the Hartmann number.

Similar computations for the duct with the FCI having a slot in the wall parallel to the magnetic field are illustrated in Fig. 5. As expected, this case

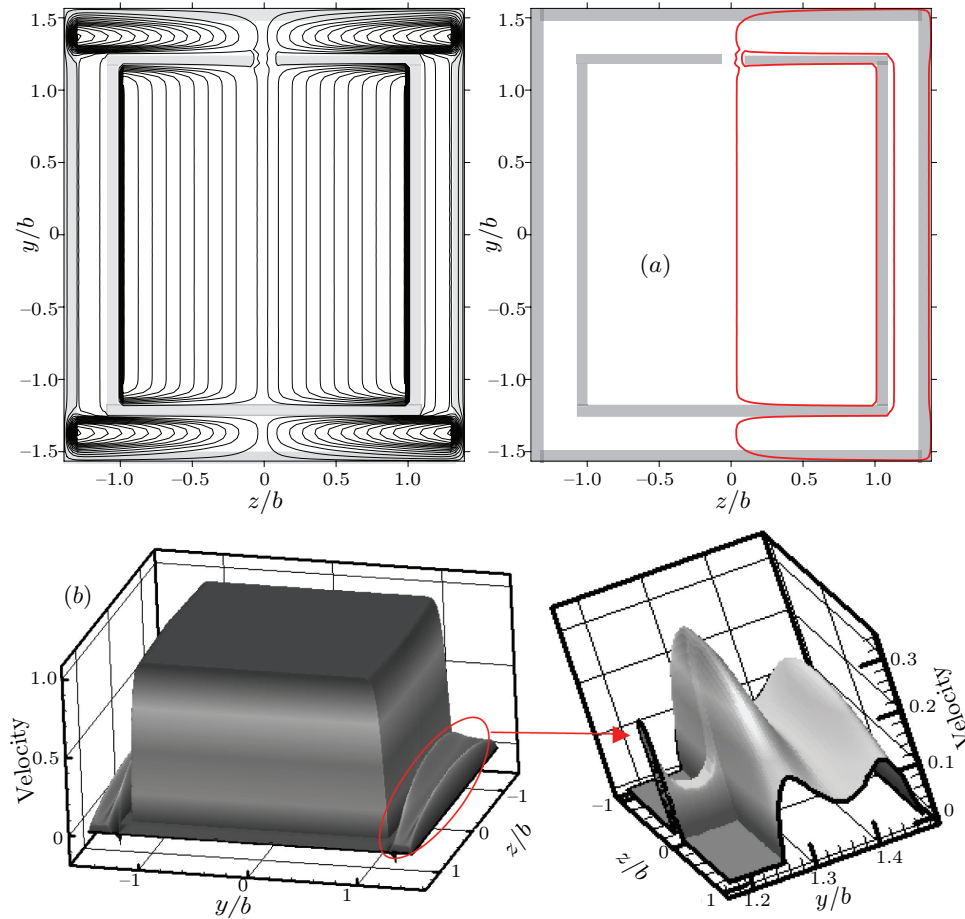
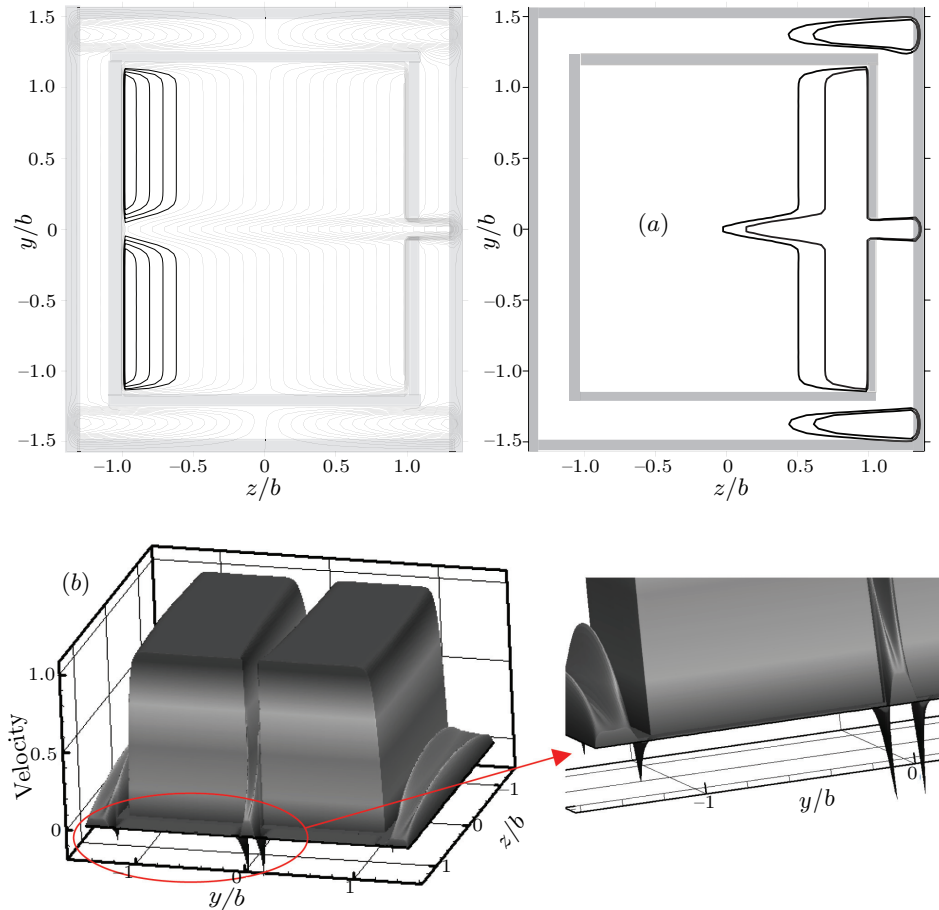


Fig. 5. Computed results for the case of the flow channel insert with the pressure equalization slot in the FCI wall parallel to the applied magnetic field: (a) induced electric current distribution, and (b) velocity distribution for  $Ha_1 = 959$  ( $B_z^0 = 1$  T).

demonstrates almost no difference with the FCI having no pressure equalization openings. There is some current leaking from the bulk flow into the gap through the opening in the FCI (Fig. 5a). This current is however very small and almost does not affect the flow distribution in the bulk and gap flows. The circuit associated with the current leaking from the bulk flow through the gap is also shown in Fig. 5. The very long current path and the associated high electric resistance explain why the leakage current is so small and why there is no any effect of the gap on the flow. This is however different from the case of the electrically conducting FCI analyzed in [4] and [10], where the electric current generated in the bulk flow crosses the FCI twice (at the top and bottom) and then passes in the wall or/and in the gap, resulting in significant changes in the velocity profile and a much higher MHD pressure drop compared to the case analyzed here.

Finally, the case with the pressure equalization slot in the FCI wall perpendicular to the magnetic field is analyzed. Again, there is some similarity in the electric current and velocity distributions with those computed in the two other cases (Fig. 6). Namely, the only one but a pronounced difference is related to the relatively small area associated with the slot. Here, formation of internal free shear layers occurs as the current leaks through the slot into the gap. In the bulk



*Fig. 6.* Computed results for the case of the flow channel insert with the pressure equalization slot in the FCI wall perpendicular to the applied magnetic field: (a) induced electric current distribution, and (b) velocity distribution for  $Ha_1 = 959$  ( $B_z^0 = 1$  T).

flow, the induced electric current in the area next to the slot turns within the shear layers at the right angle and then passes in the perpendicular direction towards the slot. Correspondingly, a velocity deficit zone in the bulk flow is formed, which stretches from the slot to the opposite wall. The thickness of the two shear layers associated with the slot seems to be proportional to  $1/\text{Ha}_1$  as these layers are similar to the Ludford layers by nature. The width of the velocity deficit zone is not constant in  $z$ ; it increases slowly with  $z$  in a parabolic manner from the slot to the opposite FCI wall. Similarly to the corner regions, the velocity profile in the overlap region, where the flow in the slot matches the gap flow, demonstrates negative velocity peaks. To our best knowledge, such negative velocity zones in fully developed flows have not been analyzed yet. It appears that formation of such negative velocity peaks occurs when two elongated core flows match at the right angle. It is not clear yet however if the presence of the electrically conducting wall is a necessary condition for the negative velocity peak formation. Regarding the MHD pressure drop, it is higher in the case with the slot in the FCI wall perpendicular to the magnetic field if compared to other two cases, where the MHD pressure drop is practically the same. For the flow parameters shown in the captions to Figs. 4, 5 and 6, the difference is only 4%. However, this difference increases as the Hartmann number increases.

**3. Experimental data and comparison with the theory.** The experiments are performed using the In-Ga-Sn loop at the Southern Institute of Physics (SWIP), China (Fig. 7). The uniform magnetic field space is 740 mm (length)  $\times$  170 mm (width)  $\times$  80 mm (height). The maximum strength of the applied (transverse) magnetic field is 2 T (maximum Hartmann number is 2400). In the test-section, the outer rectangular duct made of stainless steel is 1500 mm long, while the FCI box made of epoxy is 1 m long. The FCI is glued at the corners



*Fig. 7.* Picture of the experimental MHD facilities at the Southwestern Institute of Physics (SWIP), China.

using the same epoxy. The basic cross-sectional dimensions of the test-article are summarized in Table 1. The pressure drop is measured over a section of 500 mm long, which is well distanced from both the edges of the FCI box (250 mm apart) and the two fringing field zones at the entry to and the exit from the magnet (120 mm apart). The error of the pressure drop measurements does not exceed 3% so that the smallest pressure difference, which can be measured in the experiment, is 18.75 Pa. Pressure taps are inserted into the gap section parallel to the applied magnetic field, which faces the FCI wall without openings. This arrangement of pressure taps assumes fully developed flow conditions when the pressure is the same over the whole cross-sectional area.

Epoxy can be considered as an ideal insulator as its electric conductivity is very low,  $10^{-4}$  S/m, so that the wall conductance ratio based on the FCI thickness  $t_{\text{FCI}}$  and the half-width of the FCI box  $b$  is very small:  $t_{\text{FCI}}\sigma_{\text{FCI}}/(b\sigma_1) \sim 10^{-10}$ . The liquid metal operated at 85°C is pumped by an EM pump having a capacity of 5700 kg/h. The mass flowrate is measured by an EM flowmeter with the experimental error less than 1.3%. Along with the measurements of the MHD pressure drop, the principal experimental diagnostics allows for measurements of the electric potential at several cross-sectional locations and measurements of the velocity distribution along the duct centerline in the direction perpendicular to the applied magnetic field with the LEVI probe inserted in the liquid through the slot or a hole in the FCI. In the PES case, there are 7 equally-distanced round holes in the FCI wall parallel to the applied magnetic field, 5 mm radius each. The PEH case cannot be considered as a fully developed flow since each hole is responsible for local 3D effects, while the flow geometry independent of the axial distance in the PES case may allow the flow to become fully developed or at least about fully developed, providing the entry effects are limited to a relatively short distance of only a few duct characteristic dimensions. The transitional length associated with the entry effects can vary significantly depending on the flow velocity and magnetic field strength. That is why so far there are no strong experimental evidences confirming that the flow in the PES case within the pressure measurement section in all the experiments is fully developed.

In Fig. 8, the experimental and the computed data are plotted for the pressure drop coefficient  $\xi_2$  multiplied by the Reynolds number  $\text{Re}_2$  as a function of the Hartmann number  $\text{Ha}_2$ . The pressure drop coefficient is defined as

$$\xi_2 = -\frac{b + t_{\text{FCI}} + t_g}{\rho_l U_m^2} \frac{dp}{dx},$$

where the half-width of the outer stainless steel duct is taken as a characteristic length. The two theoretical curves in the figure are calculated for a FCI without pressure equalization openings. The upper curve represents the case when the flow channel insert and the liquid metal have the same electric conductivity. The lower curve corresponds to an ideally insulating FCI ( $\sigma_{\text{FCI}} = 0$ ). As seen, the difference in the MHD pressure drop between these two extreme cases is two orders of magnitude. The experimental MHD pressure drop coefficients for both PES and PEH cases are about one order of magnitude smaller if compared to the conducting duct. Therefore, it has been demonstrated experimentally that using the FCI can reduce the induced electric currents significantly. Of the two experimental cases, the MHD pressure drop in the PEH case is about two times smaller than that in the PES case. In all cases, the experimental MHD pressure drops are, however, higher than the computed ones using the fully developed flow model. Such a difference in MHD pressure drop between the theory and the experiment is surprisingly large indicating the need for more theoretical and experimental

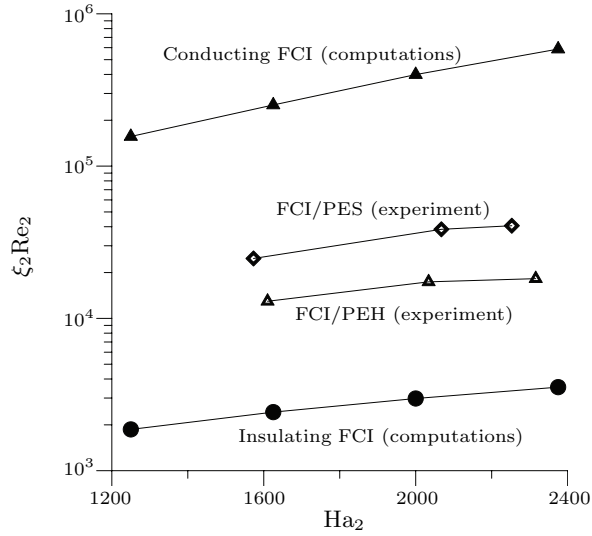


Fig. 8. Comparison of the pressure drop coefficient between the experiment and the computations.

work. In both approaches, the assumption of the fully developed flow model needs further verifications and, if needed, further corrections should be implemented, as the so-called “three-dimensional MHD pressure drop” associated with the axial electric currents in developing flows can be comparable or even higher than the MHD pressure drop associated with the cross-sectional currents in fully developed flows. Usually in simple geometry ducts without the FCI in a strong few Tesla magnetic field, the flow becomes fully developed within a short distance of a few characteristic cross-sectional duct dimensions [14]. However, in spite of the fact that in the reference experiments the pressure measurement section is spaced a few characteristic duct lengths apart from the magnet edges as well as from the edges of the FCI box, the flow can still be developing as the flow in the presence of the FCI may experience more development length. Namely, providing the pressure on both sides of the FCI is not the same, secondary flows from the bulk into the gap (or vice versa) through the pressure equalization openings seem to have a larger timescale than those in the simple geometry ducts because of the large ratio of the gap length to its width. If so, the three-dimensional effects can contribute a significant fraction to the measured MHD pressure drop making the experimental results pronouncedly different from the computed ones. These issues will be carefully addressed in the next studies. First, three-dimensional computations are planned under the experimental conditions to include flow development effects associated with the fringing magnetic field, FCI entry/exit, and to take into account the secondary flows through the pressure equalization openings. This will be done using the newly developed unstructured mesh three-dimensional MHD solver called HIMAG [15]. On the experimental part, more electric potential measurements will be taken in the axial direction to diagnose possible downstream flow variations, and the pressure drop measurements will also be performed in the bulk flow.

**Summary.** We have performed numerical computations and experiments on MHD flows in a conducting rectangular duct with a non-conducting flow channel insert in a strong (up to 2 T) steady transverse magnetic field. In the simulations, the effect of the pressure equalization openings in the form of a slot made either in the FCI wall parallel or perpendicular to the applied magnetic field has been

analyzed. We found that the PES made in the FCI wall parallel to the magnetic field had almost no effect on the flow (if compared to the case without pressure equalization openings) as all electric currents induced in the bulk flow inside the FCI box were almost not leaking outside. At the same time, the PES made in the FCI wall perpendicular to the magnetic field results in the pronounced velocity deficit zone and formation of the internal shear layers in the bulk flow similar to the Ludford layers and is responsible for a higher MHD pressure drop. In the experiment, the MHD pressure drop is measured in the In-Ga-Sn flows in a conducting rectangular duct made of stainless steel with the insulating flow insert made of epoxy, which can be considered as a perfect insulator due to its extremely low electric conductivity. Two types of pressure equalization openings both made in the FCI wall parallel to the applied magnetic field have been studied experimentally: the pressure equalization slot and the pressure equalization holes. It has been demonstrated that in all cases, the FCI has a strong effect on the flow, reducing the induced electric currents and thus the MHD pressure drop. The reduction of the MHD pressure drop in the reference MHD flows (magnetic field is from 1 to 2 T) due to the FCI is by a factor of 10 with larger reduction in the case of PEH. However, the calculated MHD pressure drop in the case of no openings or PES in the FCI wall parallel to the applied magnetic field is significantly lower (by a factor of 10) if compared to the experimental data. This discrepancy in the MHD pressure drop between the theory and the experiment may indicate some deficiency both in the theoretical approach and in the experiment. Namely, the three-dimensional effects associated with the flow development due to entry/exit effects as well as due to the secondary flows through the pressure equalization openings seem to be possible. This can result in a significant increase of the MHD pressure drop. Therefore, in the next studies, three-dimensional computations will be performed abandoning the present fully developed flow model. In the experiments, special care will be taken to diagnose the possible axial variations by measuring the electric potential distribution along the flow path and performing the pressure drop measurements in the bulk flow.

**Acknowledgments.** SS and MA acknowledge the support from the US Department of Energy through the research grant DE-FG02-86ER52123-A040. ZX and CP acknowledge the support from the National Nature Science Foundation of China through the grant 10775042.

## REFERENCES

- [1] M.S. TILLACK, S. MALANG. High Performance PbLi Blanket. In: *Proc. the 17th IEEE/NPSS Symp. Fusion Engineering* (San Diego, USA, October 6-10, 1997), vol. 2, pp. 1000–1004.
- [2] S. MALANG, E. BOJARSKY, L. BUHLER, H. DECKERS, U. FISCHER, P. NORAJITRA, H. REISER. Dual coolant liquid metal breeder blanket. In: *Proc. the 17th Symposium on Fusion Technology* (Rome, Italy, September 14–18, 1992), pp. 1424–1428.
- [3] C.P.C. WONG, S. MALANG, M. SAWAN, M. DAGHER, S. SMOLENTSEV *et al.* An overview of dual coolant Pb-17Li breeder first wall and blanket concept development for the US ITER-TBM design. *Fusion Eng. Des.*, vol. 81 (2006), pp. 461–467.
- [4] S. SMOLENTSEV, N.B. MORLEY, M. ABDU. MHD and thermal issues of the SiCf/SiC flow channel insert. *Fusion Sci. Technol.*, vol. 50 (2006), pp. 107–119.

- [5] S. SMOLENTSEV, R. MOREAU, M. ABDOU. Characterization of key magnetohydrodynamic phenomena in PbLi flows of the US DCLL blanket. *Fusion Eng. Des.*, vol. 83 (2008), pp. 771–783.
- [6] S. SMOLENTSEV, N.B. MORLEY, C. WONG, M. ABDOU. MHD and heat transfer considerations for the US DCLL blanket for DEMO and ITER TBM. *Fusion Eng. Des.*, vol. 83 (2008), pp. 1788–1791.
- [7] C. MISTRANGELO, A.R. RAFFRAY, AND THE ARIES TEAM. MHD analysis of dual coolant Pb-17Li blanket for ARIES-CS. *Fusion Sci. Technol.*, vol. 52 (2007), pp. 849–854.
- [8] L. BARLEON, V. CASAL, K.J. MACK, H. KREUZINGER, A. STERL, K. THOMASKE. *Experimental and theoretical work on MHD at the Kernforschungszentrum Karlsruhe. The Mekka Program* (Liquid Metal Magnetohydrodynamics, Mech. of Fluids and Transport Processes, vol. 10, Kluwer Acad. Publ., 1989), pp. 55–61.
- [9] Z. XU, C. PAN, X. ZHANG, L. ZHAO, J. ZHANG, G. YANG. Primary experimental results of MHD flow in the duct with flow channel insert. *Nuclear Fusion and Plasma Physics*, vol. 29 (2009), pp. 6–9 (in Chinese).
- [10] S. SMOLENTSEV, N. MORLEY, M. ABDOU. Code development for analysis of MHD pressure drop reduction in a liquid metal blanket using insulation technique based on a fully developed flow model. *Fusion Eng. Des.*, vol. 73 (2005), pp. 83–93.
- [11] J.C.R. HUNT. Magnetohydrodynamic flow in rectangular ducts. *J. Fluid Mech.*, vol. 21 (1965), pp. 577–590.
- [12] G.S.S. LUDFORD. The effect of a very strong magnetic cross-field on steady motion through a slightly conducting fluid. *J. Fluid Mech.*, vol. 10 (1960), pp. 141–155.
- [13] J.C.R. HUNT, S. LEIBOVICH. Magnetohydrodynamic flow in channels of variable cross-section with strong transverse magnetic fields. *J. Fluid Mech.*, vol. 28 (Part 2), pp. 241–260.
- [14] J.H. DAVIDSON, F.A. KULACKI. *Convective heat transfer with electric and magnetic fields* (Handbook of Single-Phase Convective Heat Transfer. Edited by S. Kakac, R.K. Shah, W. Aung. John Willey & sons, 1987).
- [15] R. MUNIPALLI *et al.* *Development of a 3-D incompressible free surface MHD computational environment for arbitrary geometries: HIMAG* (DOE SBIR Phase-II Final Report, June 2003).

Received 27.07.2009